


Simulation of actin distribution of osteoblasts on titanium pillar arrays using a bio-chemo-mechanical model

D. Truong¹  | C. R. Bahls¹ | B. Nebe² | U. van Rienen¹

¹Institute of General Electrical Engineering, University of Rostock, Albert-Einstein-Str. 2, Rostock 18059, Germany

²Department of Cell Biology, University Medical Center Rostock, Schillingallee 69, Rostock 18057, Germany

Correspondence

D. Truong, Institute of General Electrical Engineering, University of Rostock, Albert-Einstein-Str. 2, Rostock 18059, Germany.
Email: duy.truong@uni-rostock.de

Funding information

Deutsche Forschungsgemeinschaft, Grant/Award Number: GRK 1505/2

Abstract

A numerical model for the adhesion of osteoblasts on titanium micropillar structures is suggested, and a function representing the concentration level of the adhesion on the pillars is constructed based on experimental observation. The introduction of this function helps a well-known bio-chemo-mechanical model to better predict the formation of actin in osteoblasts when they are laid on arrays of titanium micro-pillars of various size attached to silicon substrate. A parameter study suggests that each pillar is associated with a different pattern of adhesion. Our finding emphasises a capability of the bio-chemo-mechanical model that it can well explain the strong influence of the boundary condition on the formation of actin within the cells.

KEYWORDS

actin distribution, bio-chemo-mechanical model, computational modelling, osteoblasts-substrate interaction

1 | INTRODUCTION

Knowledge about the interaction between bone cells and their surrounding biomaterials is essential for the improvement in quality of an implant. Numerous experiments have been done to measure mechanical interactions between cells and the underlying substrates. Well-known methods include those introduced by Harris et al,¹ Burton and Taylor,² and Balaban et al.³ A more efficient method was introduced by Tan et al,⁴ in which cells are laid on a bed of microneedles so that forces exerted by cells can be measured from the individual displacements of the needles. This method was widely applied and adapted to achieve further understanding on behaviour of the cells. For example, Sniadecki et al⁵ used magnetic and nonmagnetic posts to apply external forces and monitor traction forces. Matschegewski et al⁶ investigated the difference in actin cytoskeleton organization of bone cells when they are laid on a planar surface and cubic micropillar structures of different dimensions, respectively.

Besides experiments, numerical modelling has been a good approach to understand mechanisms of the mechanical interaction between cells and the underlying substrate. Several numerical models with different complexities have been developed to simulate the contractility of cells and the organisation of the stress fibres. Examples of existing models are those introduced by Storm et al,⁷ Satcher and Dewey,⁸ Mohrdieck et al,⁹ Nelson et al¹⁰ and Sanz-Herrera et al.¹¹ These models are either passive models, where the cell contractility is not included, or active models—yet neglecting the biochemical cause of the active cell response.

The bio-chemo-mechanical (BCM) model proposed by Deshpande et al¹² is known as being advantageous compared with other numerical models, as it includes the biochemical processes and can efficiently explain many effects such

.....
This is an open access article under the terms of the Creative Commons Attribution-NonCommercial License, which permits use, distribution and reproduction in any medium, provided the original work is properly cited and is not used for commercial purposes.

© 2018 The Authors International Journal for Numerical Methods in Biomedical Engineering Published by John Wiley & Sons Ltd.

as the strong dependence of the forces generated by the cells on the substrate compliance as well as the influence of boundary conditions on the orientation and formation of stress fibres. This model was inspired by the experiments of Tan et al,⁴ where smooth muscle cells were laid on beds of microneedles, and was developed based closely on experimental observations. According to Deshpande et al,¹³ their model was motivated by several key biochemical processes. One of the involved processes is the activation of myosin II. When a phosphorylation occurs, possibly by light-chain kinase or by Rho-kinase, the myosin II tends to take the active extended state. The extended myosins associate to form bipolar filaments, which later enter between the actin filaments bundled together by α actinin to form contractile stress fibres.¹³

By addressing the biochemical processes, the BCM model is more realistic compared with passive models. Moreover, a full interpretation of experimental data on forces generated by living cells can only be obtained in appropriate constitutive models, where the active response of cells is included.¹³ Because of its efficiency, the BCM model has been widely applied in modelling the contractile response and actin distribution in cells of different types. McGarry et al¹⁴ used this model to simulate the behaviour of smooth muscle cells and other cell lines, such as fibroblasts, on beds of microposts. Together with a biochemical model for focal adhesion,¹⁵ this model has been used to simulate the concentration of actin in the cell and of integrins at the contact regions.^{16,17} An application to a 3-dimensional cell structure was done by Dowling et al.¹⁸

The aim of this paper is to apply the BCM model to predict the tendency for the concentration of actin in osteoblasts observed in the experiments of Matschegewski et al,⁶ where they were laid on arrays of regular titanium pillars attached to silicon substrates. It is revealed from the experimental results that for osteoblasts, actin was distributed in short fibres on the titanium pillar structure, while in the experiments of Tan et al⁴ for smooth muscle cells, actin was found as long fibres distributed intensely around the pillars. Therefore, simply applying the approach of McGarry et al,¹⁴ which was derived for smooth muscle cells, will not be feasible. We will propose a set of parameters and a hypothesis for inhomogeneous adhesion and show that the BCM model can really help predict the tendency of the osteoblast actin distribution.

2 | THE MODEL

2.1 | The BCM model

The BCM model¹² is defined for a single stress fibre and is described by 3 equations. First, by ignoring the details of the signalling processes, a simple exponential function $C(t) = \exp(-t/\theta) \in [0, 1]$ is used to represent the time dependency of the level of an external signal C . Here, θ is the decay constant of a chemical compound; t is the time measured from the instant of the most recent signal. Second, a nondimensional activation level $\eta \in [0, 1]$ is introduced to describe the remodelling of actin cytoskeleton under external stress. Based on experimental observations, the equation for evolution of η is established as

$$\dot{\eta} = [1 - \eta] \frac{C \bar{k}_f}{\theta} - \left[1 - \frac{\sigma}{\sigma_0} \right] \eta \frac{\bar{k}_b}{\theta}, \quad (1)$$

where the term $[1 - \eta] \frac{C \bar{k}_f}{\theta}$ expresses the rate of stress-fibre-formation dependent on the signal C and is controlled by the constant \bar{k}_f . Similarly, the second term on the right-hand side is a non-negative number that expresses the rate of stress fibre dissociation, which depends on the current tension relative to the isometric tension σ_0 and is controlled by the constant \bar{k}_b . Here, σ_0 is the maximum tension allowed in the stress fibre corresponding to the activation level η and is given as $\sigma_0 = \eta \sigma_{\max}$, where σ_{\max} is the maximum tension at $\eta = 1$, that is, when the stress fibre is fully activated. Finally, a linearised Hill equation¹⁹ is used to describe the relationship between tension σ and the lengthening/shortening strain rate $\dot{\epsilon}$ as

$$\frac{\sigma}{\sigma_0} = 1 + \frac{\bar{k}_v}{\eta} \left(\frac{\dot{\epsilon}}{\dot{\epsilon}_0} \right), \quad (2)$$

where \bar{k}_v is the fractional reduction in fibre stress upon increasing the shortening rate relative to $\dot{\epsilon}_0$. This linearised relation is described in Han and Sniadecki²⁰ and Rodriguez et al.²¹ When the cells are considered as continuous medium, the theory of continuum mechanics can be used, and the BCM model is included by introducing an active stress tensor S^{active} so that the total stress in the cell is obtained as

$$S^{\text{total}} = S^{\text{active}} + S^{\text{passive}}, \quad (3)$$

where S^{passive} is the passive stress due to the cell material and depends on the material model used. For example, when it is assumed that the cell behaviour is linearly elastic and the deformation can be large, then S^{passive} becomes the second Piola-Kirchhoff stress tensor and is related to the Green-Lagrange strain tensor E by $S^{\text{passive}} = C : E$, where C is the

stiffness tensor and the colon ($:$) denotes the double contraction of the 2 tensors. To obtain the active stress S^{active} , first, the possible directions for stress fibres at each point in the cell need to be defined. In 2-dimensional analysis, the stress fibres are assumed to be able to form uniformly in all directions. Each direction is determined by the angle ϕ between the fibre and the e_1 axis. The unit vector for this direction is $m(\phi) = \cos(\phi)e_1 + \sin(\phi)e_2$. The strain rate $\dot{\epsilon}$ in Equation 2 of the stress fibre in the direction $m(\phi)$ is calculated from the material strain rate \dot{E} as

$$\dot{\epsilon} = \dot{E}_{11}\cos^2\phi + \dot{E}_{22}\sin^2\phi + \dot{E}_{12}\sin 2\phi. \quad (4)$$

Because of symmetry, the components of the average active stress tensor in Cartesian coordinates are obtained as

$$S_{ij}^{\text{active}} = \frac{1}{\pi} \int_{-\pi/2}^{\pi/2} \sigma(\phi)m_i(\phi)m_j(\phi)d\phi \quad i, j = 1, 2, \quad (5)$$

where σ is the tension in the stress fibre (in Equation 2). The active stress tensor is written as

$$S^{\text{active}} = \begin{pmatrix} S_{11}^{\text{active}} & S_{12}^{\text{active}} \\ S_{21}^{\text{active}} & S_{22}^{\text{active}} \end{pmatrix} = \frac{1}{\pi} \int_{-\pi/2}^{\pi/2} \begin{pmatrix} \sigma(\phi)\cos^2\phi & \sigma(\phi)\sin\phi\cos\phi \\ \sigma(\phi)\sin\phi\cos\phi & \sigma(\phi)\sin^2\phi \end{pmatrix} d\phi. \quad (6)$$

In finite element analysis, the above integral can only be calculated numerically. Deshpande et al¹³ suggested that a large number N_d directions for stress fibres should be defined by spacing equally N_d angles $\phi \in [-\pi/2, \pi/2]$ and the trapezoidal rule over these sampling points can be used to obtain the integrals. We have introduced an alternative approach, where a quadratic function is used to approximate the activation level, and obtained similar results while a significant improvement in computing time is achieved.²²

2.2 | Measure for actin distribution

When the activation level in the cell is obtained, there is a measure that is shown by McGarry et al¹⁴ to be corresponding to the patterns of actin distribution. This measure is defined as

$$\Pi = \eta_{\max} - \bar{\eta}, \quad (7)$$

where η_{\max} is the maximum activation and $\bar{\eta}$ is the average activation in all directions. For 2D analysis, $\bar{\eta}$ is written as $\bar{\eta} = (1/\pi) \int_{-\pi/2}^{\pi/2} \eta(\phi)d\phi$ and is also computed numerically.

2.3 | Inhomogeneous cell adhesion

It revealed from the experiments of Matschegewski et al⁶ that cell adhesion was not completely uniform in the contact region between the cell and the top of the pillars. The adherence was nearly homogeneous, but spot adherence existed on top of the pillars. To model this inhomogeneity of the adhesion, we used a scaling function $g(x, y)$, whose value is in the range $[0, 1]$, to represent the concentration level of the adhesion on a single pillar. The value 1 is assigned to the regions where spot adherence occurs, while the zero value indicates the disappearance of the adhesion. The pillars are assumed to have square shape with blunt corners, which are close to those used in the experiments of Matschegewski et al.⁶ For simplicity and from the observation that spot adherence usually appeared near the periphery of the pillars, especially the corners, we constructed a smooth function that holds a small value everywhere except for the regions near the 4 corners of the pillar. The left part of Figure 1 displays a possible choice for our function, while the right figure shows the 1D plot of a slice through 2 spots. With s being the side of the pillar and we denote

$$f(x) = \frac{1}{2} \left(\cos \left(6\pi \frac{x - 0.5s}{0.9s} \right) + 1 \right) \in [0, 1], \text{ for } x \in [0, s], \quad (8)$$

the expression for the adhesion level that we used is

$$g(x, y) = \begin{cases} \frac{9}{10} f(x) * f(y) + \frac{1}{10}, & \text{if } |x - 0.5s|, |y - 0.5s| \in [0.15s, 0.45s] \\ \frac{1}{10}, & \text{otherwise} \end{cases} \quad (9)$$

for $(x, y) \in [0, s] \times [0, s]$ representing a point on the pillar structure. The values of the function g are in the range $[0.1, 1]$. This is equivalent to the assumption that the adhesion at the peak points is 10 times stronger than that at those points

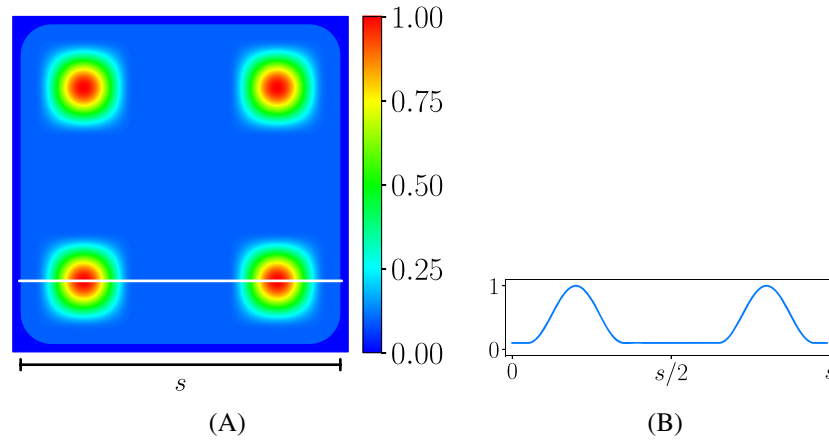


FIGURE 1 Plot of an exemplary function for the concentration level of the adhesion on a single pillar and plot of a slice through 2 spots. Outside of the pillar, the function vanishes. Maximal function values are reached near the 4 corners of the pillar

where the strength of adhesion is lowest. When desired, the function can easily be adjusted to meet other assumptions. The simple adhesion model in McGarry et al¹⁴ is then modified so that the traction in the cell at the contact region becomes

$$T_i = g(x, y) \cdot k_t \cdot \Delta_i, \quad (10)$$

where k_t is the shear stiffness constant of the adhesion, when the cell moves a distance Δ_i from the pillar.

Our successful formulation for the inhomogeneous adhesion between cells and the substrate leads to several possible extensions and applications of the model. First, besides in vitro experiments, in silico simulation can be performed to investigate the dependency of the patterns of actin in osteoblasts on the geometry of each pillar and of the pillar array. Second, a framework for the dynamics of focal adhesion can be developed. Such framework already exists in literature, for example, the work of Deshpande et al¹⁵ that based on thermodynamic equilibrium of the integrins. However, the appearance of adhesion spots as in the experiments of Matschegewski et al⁶ cannot be captured. Our formulation provides an insight for the improvement of such model and the achievement of a complete model that can simultaneously characterise the development of the focal adhesions and the formation of stress fibres in cells of different types. Finally, the appropriateness of the BCM model in modelling the actin formation in osteoblasts is confirmed. With the set of parameters we obtained, the model can be used to numerically study the behaviour of osteoblasts in other experimental set-ups. For example, the study of the dynamics of traction forces in osteoblasts under effects of exposure to external electric fields, which has been studied experimentally by Curtze et al,²³ can be performed.

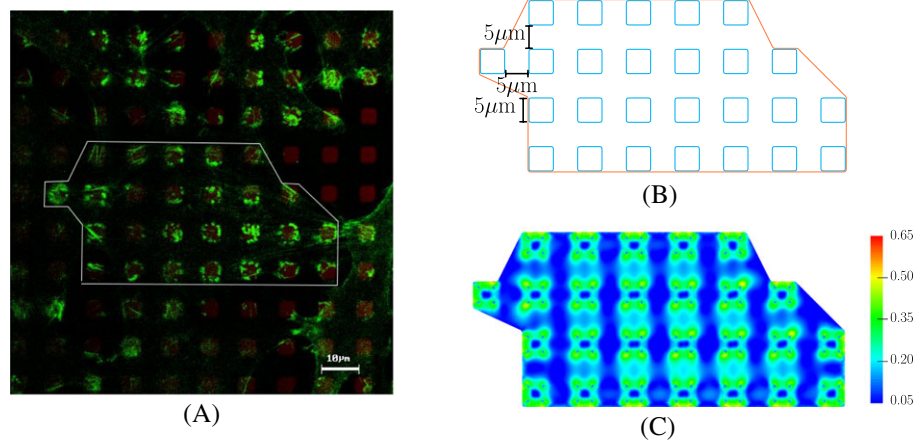
3 | RESULTS AND DISCUSSION

We apply the BCM model together with our suggested model for the adhesion of the cell to the pillar structure to simulate the actin distribution of osteoblasts on titanium arrays of different dimensions. The parameters for the BCM model, the material properties of the pillars, and the passive mechanical material properties of the cell are shown in Table 1. The values for θ , \bar{k}_f , \bar{k}_b , and \bar{k}_v are the same as those in McGarry et al.¹⁴ From experimental observation, we know that osteoblasts generate a very small contraction force. Thus, the values that we used for σ_{\max} and $\dot{\epsilon}_0$ are $0.15 \text{ [nM}/\mu\text{m}^2]$ and $10^{-5} \text{ [s}^{-1}]$, respectively, are much smaller than the values in McGarry et al.¹⁴ At the regions where the cell is in contact with the pillars, the value $k_t = 500 \text{ nM}/\mu\text{m}^3$ is used for the focal adhesion stiffness, which is also the same as that in McGarry et al,¹⁴ and Equation 10 is used for the shear traction.

The system of governing equations, which includes the equilibrium condition and Equation 1, is solved using finite element analysis. Since almost no deflection of the pillars was found in the experiments, the usual approach is considering the pillars as rigid bodies and applying a homogeneous Dirichlet boundary condition. Here, we used the approach in McGarry et al¹⁴ and modelled the pillars as rounded rectangular surfaces connected to springs of a large stiffness. This relaxation allows the stability of the solution procedure, while the obtained displacement of the pillars is small enough to be ignored. The linear elastic material model is used for both the cell and the pillars.

TABLE 1 Parameters for the BCM model, material properties of the pillars, and passive mechanical properties of the cell

Parameter	Value	Description
σ_{\max}	0.15 [nN/ μm^2]	maximum fibre tension
θ	70 [s]	Decay constant of signal
\bar{k}_v	7	Tension reduction coefficient with respect to strain rate
\bar{k}_f	10	Formation rate constant
\bar{k}_b	1	Dissociation rate constant
$\dot{\epsilon}_0$	10^{-5} [s^{-1}]	Initial fibre contraction rate
k_t	500 [nN/ μm^3]	Focal adhesion stiffness
E_{cell}	0.4 [nN/ μm^2]	Young modulus of the cells
ν_{cell}	0.3	Poisson ratio of the cells
E_{pillar}	$1.0 \cdot 10^3$ [nN/ μm^2]	Young modulus of the pillars
ν_{pillar}	0.35	Poisson ratio of the pillars

**FIGURE 2** Experimental and predicted distributions of actin in osteoblasts. A, Fluorescence image of the actin filament distribution in MG-63 osteoblasts (actin in green, LSM 780, bar 10 μm ; with courtesy of H. Rebl). The white line demonstrates a simplified form of 1 cell. The cell lies on several micropillars. B, Sketch of the patch of 1 cell used in the simulation. C, Our predicted result for actin distribution (characterised by the measure Π) using the bio-chemo-mechanical model and our description for the cell-pillar adhesion

We used the *gms*h generator²⁴ to create the meshes and the open source framework *FEniCS*, version 2016.2, to compute the solution.²⁵ For time discretisation, we used an explicit method with a maximum time step of 2 seconds and performed a convergence study to make sure that the solution is stable with our choice of time step.

To demonstrate the applicability of our model using an inhomogeneous adhesion function, we conducted the simulations for osteoblasts on arrays of square pillars of different sizes: $5\mu\text{m} \times 5\mu\text{m}$ and $3\mu\text{m} \times 3\mu\text{m}$. For simplicity, we used the same function $g(x, y)$ (Equation 9) for the adhesion at all pillars.

3.1 | Osteoblasts on titanium coated pillars of $5\mu\text{m} \times 5\mu\text{m}$

We first apply the model to a cell patch on 26 pillars in our experiment, as shown in Figure 2A. We constructed a cell geometry with the assumption that the initial cell has straight edges between pillars and it fits perfectly to the 26-pillar subarray depicted in Figure 2B. Moreover, we also assume that the pillars are of perfect square shape with blunt corners. The side length of the pillars is $5\mu\text{m}$, while the radius of the corner fillet is $0.5\mu\text{m}$ (area $\approx 24.77\mu\text{m}^2$). The distance between 2 neighbouring pillars is also $5\mu\text{m}$. The height of each pillar is $5\mu\text{m}$, but this value is not incorporated in the model, since the pillars are represented by top surfaces connected to springs.¹⁴ We used the value $7.5\text{nN}/\mu\text{m}$ for the spring stiffness, which is high enough for the pillar displacement to be close to zero as in the experiments.

The simulation result for actin formation is shown in Figure 2C. It can be seen that on the pillars, the actin is of highest amount, and it is distributed nonuniformly. Moreover, at the longest edges of the cell, there is more actin than at other

edges. The obtained maximum displacement of the pillars is around $7\mu\text{m}$, which is 0.14% of the side length of the pillar. Analogous outcome is achieved when we apply the model for an osteoblast on an array of 19 pillars, which is illustrated in Figure 3.

It should be noted that without our adaptation of the model for the adhesion of muscle cells to the adhesion of osteoblasts involving an inhomogeneous adhesion behaviour, the result would not agree with the experiment, as the predicted actin would form around the pillars, and there would be a uniform low level of actin on the pillars (Figure 3). To further improve the agreement between the results using our approach, the complexity of the model should be increased: A more complex function $g(x, y)$ for the adhesion should be constructed, and the function could also be different for each pillar.

3.2 | Osteoblasts on titanium coated pillars of $3\mu\text{m} \times 3\mu\text{m}$

Similar steps are applied for the simulation of osteoblasts on an array of pillars of dimension $3\mu\text{m} \times 3\mu\text{m}$. The radius for the rounded corners is chosen to be $0.4\mu\text{m}$, and the distance between 2 neighbouring pillars is $3\mu\text{m}$, as in the experiment in Matschegewski et al.⁶ As the area of the pillar is around $8.85\mu\text{m}^2$, which is smaller than that in the previous example, the corresponding spring stiffness is set to $2.68\text{ nN}/\mu\text{m}$.

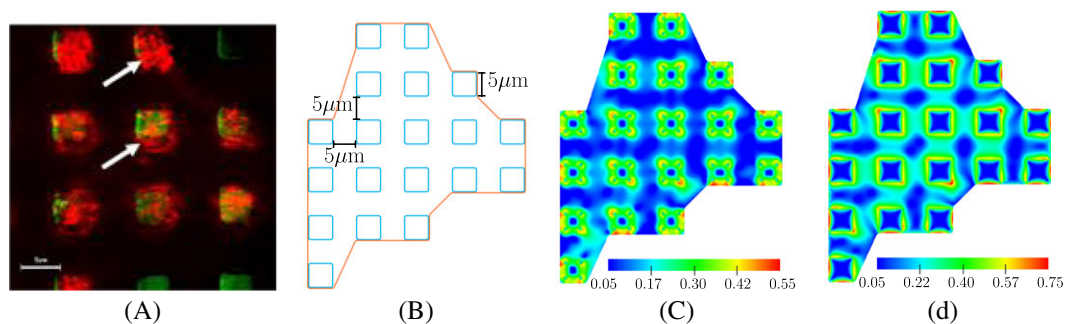


FIGURE 3 Experimental and predicted distributions of actin in osteoblasts. A, Experimental result for the actin distribution of a MG-63 osteoblast on a $5\mu\text{m} \times 5\mu\text{m}$ pillar array by Matschegewski et al.⁶ B, Sketch of the cell used in our simulation. C, Our simulation result for steady state actin distribution in this cell using our scaling function for inhomogeneous adhesion. D, Simulated steady state actin distribution when a homogeneous adhesion was used. The simulated actin distribution is characterised by the measure Π in Equation 7

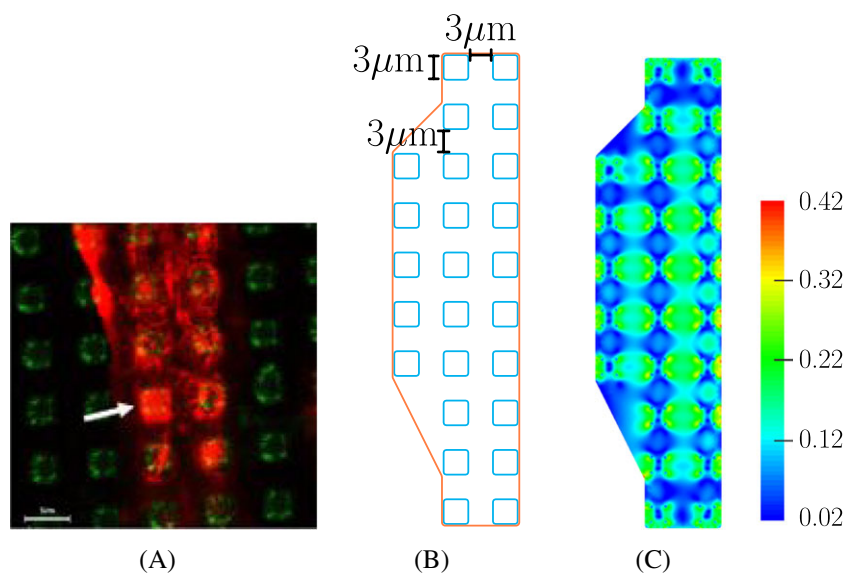


FIGURE 4 Experimental and predicted distributions of actin in osteoblasts. A, Actin formation of MG-63 osteoblasts on $3\mu\text{m} \times 3\mu\text{m}$ pillar array as described by Matschegewski et al.⁶ B, Sketch of the cell used in our simulation. C, Our predicted actin distribution characterised by the measure Π in Equation 7

The predicted actin distribution is shown in Figure 4. As in the previous case, the highest concentration of actin is located on the pillars. Since the distance between the pillars is small, a relatively high level of actin can also be found in the parts of the cell connecting the pillars. In the experiment, at some regions, the actin concentration in those parts is similar to that on the pillars.

3.3 | Effect of the adhesion scaling function

To study numerically the dependency of actin patterns on the adhesion between the cell and the pillars, we constructed different configurations for our adhesion scaling function. We varied the location and the area of strong adhesion near the peak points. We also used different number of peak points on each pillar. Examples of our adhesion scaling functions defined on a single pillar are shown in Figure 5.

Using these scaling functions for the adhesion, we performed the analysis for the actin distribution of an osteoblast on an array of 19 pillars of $5\mu\text{m} \times 5\mu\text{m} \times 5\mu\text{m}$. It can be seen from the analysis results, which are shown in Figures 3 and 6, that changing the size of the peak adherence does not affect much the trend of the actin formation on the pillars. However, the small area of these peak points gives a more smooth actin distribution. Modifying the number of peak points could deliver a different pattern of actin on the pillars, where the amount of actin is affected. We also performed a simulation in which a mix of the 4 scaling functions were used. The result in Figure 7 supports our suggestion that using different scaling functions for different pillars could give a better agreement between simulation and experimental results.

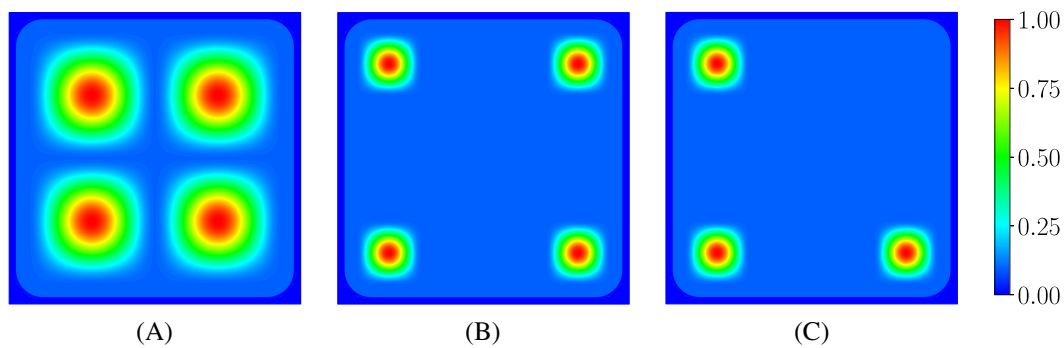


FIGURE 5 Different adhesion scaling functions for 1 single pillar. A, the strongest adhesions locate at 4 spots with a large area distributed uniformly on the pillar. B and C, peak adhesions are at 4 and 3 spots, respectively, with a small area distributed near the corners of each pillar. The functions are obtained by a slight modification of Equations 8 and 9

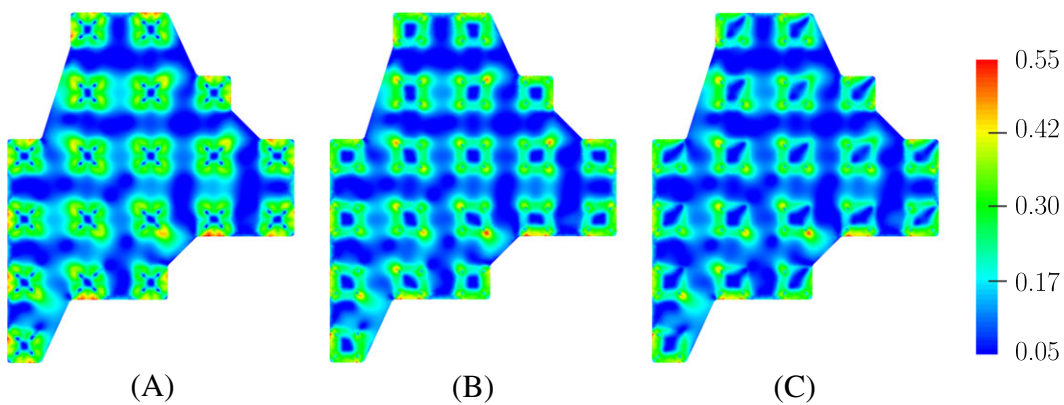


FIGURE 6 Predicted results for actin distribution of an osteoblast on an array of 19 pillars using different adhesion scaling functions. Each function is applied for all 19 pillars in every simulation

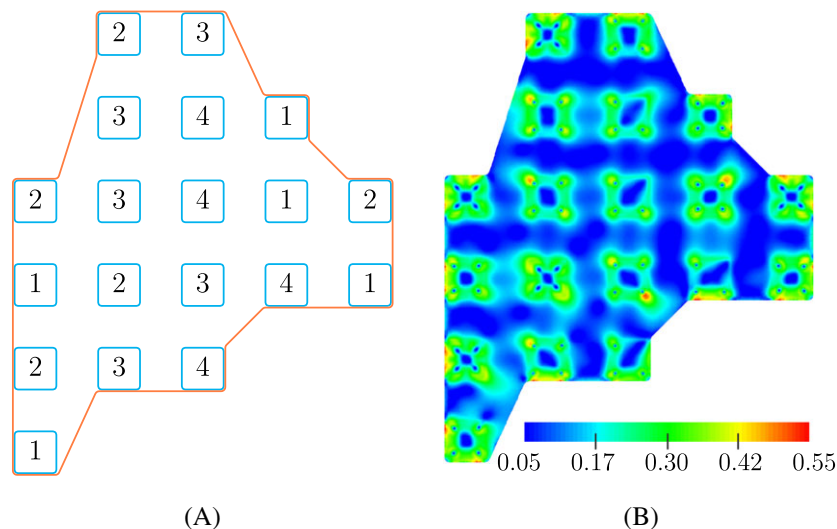


FIGURE 7 Predicted results for actin distribution of an osteoblast on an array of 19 pillars. A, Sketch of an osteoblast on 19 pillars with different adhesion patterns and B, predicted result for the actin distribution obtained in our simulation. A, 1 indicates the adhesion pattern in Figure 1A, while 2, 3, and 4 express the patterns illustrated in Figure 5A-C, respectively

4 | CONCLUSION

We have described a computational model that can predict the distribution of actin in osteoblasts when they are laid on arrays of titanium micropillars. Our model was based on the BCM model of Deshpande et al.¹²

The BCM model proposed by Deshpande et al.¹² has the capability to simulate the contractility and actin formation of biological cells when they are laid on different kinds of substrate. By including the biochemical processes, this model is more realistic than many passive models and other active models. The efficiency of this model has been shown through its applications in a great number of researches. Using this model and a simple model for the adhesion between cell and the substrate, McGarry et al.¹⁴ successfully simulated the actin distribution in smooth muscle cells and fibroblasts on arrays of polydimethylsiloxane posts. Direct application of the approach of McGarry et al to the experiments with osteoblasts on titanium micropillar arrays would lead to a great disagreement between experimental and simulated results. We suggested that this disagreement was caused by the behaviour of the contact between osteoblasts and the micropillars. We proposed a mathematical model for inhomogeneous adhesion and constructed a function that represents the concentration of adhesion on a pillar: The adhesion is locally strong at a few points near the pillar corners, and it is weaker and almost homogeneous at the remaining area. We demonstrated our approach by applying it to our experiments and to previous experimental results by Matschegewski et al.⁶ Our finding supports the appropriateness of the BCM model and reconfirms its feature that it is able to capture the strong influence of the boundary condition on the formation of actin within the cells.

ACKNOWLEDGEMENTS

This work was supported by the German Science Foundation (DFG) in the scope of the Research Training Group GRK 1505/2 “Analysis and simulation of electrical interactions of implants with bio-systems”—*welisa*. The support is gratefully acknowledged.

ORCID

D. Truong  <http://orcid.org/0000-0003-0941-9388>

REFERENCES

1. Harris AK, Stopak D, Wild P. Fibroblast traction as a mechanism for collagen morphogenesis. *Nature*. 1981;290:249-251.
2. Burton K, Taylor DL. Traction forces of cytokinesis measured with optically modified elastic substrata. *Nature*. 1997;385:450.

3. Balaban NQ, Schwarz US, Riveline D, et al. Force and focal adhesion assembly: a close relationship studied using elastic micropatterned substrates. *Nature Cell Biology*. 2001;3:466-472.
4. Tan JL, Tien J, Pirone DM, Gray DS, Bhadriraju K, Chen CS. Cells lying on a bed of microneedles: an approach to isolate mechanical force. *Proc Natl Acad Sci USA*. 2003;100:1484-1489.
5. Sniadecki NJ, Anguelouch A, Yang MT, et al. Magnetic microposts as an approach to apply forces to living cells, Vol. 104; 2007:14553-14558.
6. Matschegewski C, Staehle S, Loeffler R, et al. Cell architecture-cell function dependencies on titanium arrays with regular geometry. *Biomaterials*. 2010;31:5729-5740.
7. Storm C, Pastore JJ, MacKintosh FC, Lubensky TC, Janmey PA. Nonlinear elasticity in biological gels. *Nature*. 2005;435(7039):191-400.
8. Satcher RLJ, Dewey CFJ. Theoretical estimates of mechanical properties of the endothelial cell cytoskeleton. *Biophys J*. 1996;71(1):109-118.
9. Mohrdieck C, Wanner A, Roos W, et al. A theoretical description of elastic pillar substrates in biophysical experiments. *Chem Phys Chem*. 2005;6(8):1492-1498.
10. Nelson CM, Jean RP, Tan JL, et al. Emergent patterns of growth controlled by multicellular form and mechanics. *Proc Natl Acad Sci USA*. 2005;102(33).
11. Sanz-Herrera JA, Moreo P, Garcia-Aznar JM, Doblare M. On the effect of substrate curvature on cell mechanics. *Biomaterials*. 2009;30(34):6674-6686.
12. Deshpande VS, McMeeking RM, Evans AG. A bio-chemo-mechanical model for cell contractility. *Proc Natl Acad Sci USA*. 2006;103:14015-14020.
13. Deshpande VS, McMeeking RM, Evans AG. A model for the contractility of the cytoskeleton including the effects of stress-fibre formation and dissociation. *Proc R Soc A*. 2007;463:787-815.
14. McGarry JP, Fu J, Yang MT, et al. Simulation of the contractile response of cells on an array of micro-posts. *Proc R Soc A*. 2009;367:3477-3497.
15. Deshpande VS, Mrksich M, McMeeking RM, Evans AG. A bio-mechanical model for coupling cell contractility with focal adhesion formation. *J Mech Phys Solids*. 2008;56(4):1484-1510.
16. Ronan W, Deshpande VS, McMeeking RM, McGarry JP. Cellular contractility and substrate elasticity: a numerical investigation of the actin cytoskeleton and cell adhesion. *Biomech Model Mechanobiol*. 2014;13(2):417-435.
17. Pathak A, Deshpande VS, McMeeking RM, Evans AG. The simulation of stress fibre and focal adhesion development in cells on patterned substrates. *J R Soc Interface*. 2008;5(22):507-524.
18. Dowling EP, Ronan W, Ofek G, et al. The effect of remodelling and contractility of the actin cytoskeleton on the shear resistance of single cells: A computational and experimental investigation. *J R Soc Interface*. 2012;9(77):3469-3479.
19. Hill AV. The heat of shortening and the dynamic constants of muscle. *Proc. R. Soc. B*. 1938;126(843):136-195.
20. Han SJ, Sniadecki NJ. Simulations of the contractile cycle in cell migration using a bio-chemical-mechanical model. *Computer Methods in Biomechanics and Biomedical Engineering*. 2011;14(5):459-468.
21. Rodriguez ML, McGarry PJ, Sniadecki NJ. Review on cell mechanics: experimental and modeling approaches. *Appl Mech Rev*. 2013;65(6):060801-1-060801-41.
22. Bahls C, Truong D, van Rienen U. Semi-analytical representation of the activation level in stress fibre directions as alternative to the angular representation in the bio-chemo-mechanical model for cell contractility. *J Mech Behav Biomed Mater*. 2018;77:527-533.
23. Curtze S, Dembo M, Miron M, Jones DB. Dynamic changes in traction forces with DC electric field in osteoblast-like cells. *J Cell Sci*. 2004;117(13):2721-2729.
24. Geuzaine C, Remacle JF. Gmsh: A 3-d finite element mesh generator with built-in pre- and post-processing facilities. *Int J Numer Methods Eng*. 2009;79(11):1309-1331.
25. Logg A, Mardal KA, Wells GN, et al. *Automated Solution of Differential Equations by the Finite Element Method*. Springer; 2012.

How to cite this article: Truong D, Bahls CR, Nebe B, van Rienen U. Simulation of actin distribution of osteoblasts on titanium pillar arrays using a bio-chemo-mechanical model. *Int J Numer Meth Biomed Engng*. 2018;34:e3097. <https://doi.org/10.1002/cnm.3097>